ΠΡΑΚΤΙΚΑ ΤΗΣ ΑΚΑΔΗΜΙΑΣ ΑΘΗΝΩΝ

ΣΥΝΕΔΡΙΑ ΤΗΣ 13ΗΣ ΝΟΕΜΒΡΙΟΥ 1997

ΠΡΟΕΔΡΙΑ ΝΙΚΟΛΑΟΥ ΜΑΤΣΑΝΙΩΤΗ

ΜΗΧΑΝΙΚΗ. — **Multiaxial Failure Strength of Polycrystalline Ice I,** by Academician *Pericles S. Theocaris**.

ABSTRACT

An experimental investigation was undertaken for evaluating the failure mode of polycrystalline granular fresh-water ice at temperatures around -20° C. A series of triaxial compression tests, where the secondary lateral stresses σ_1 and σ_2 were taken always equal to each other and their magnitude did not overpass a limit of 0.50 σ_3, were used as data for determining the failure locus of this material. The experimental data corresponding to the initial, as well as to subsequent yield loci, were introduced to an appropriate tensor failure polynomial criterion, suitable for defining failure loci for anisotropic materials. Based on modern connectionistic theories, we approximated the anisotropic hardening elastoplastic behavior of the ice by a fictitious appropriate anisotropic elastic material, whose properties are adapted to the existing data of the tests in the elastoplastic range of loading. These data were used as the input values into an elliptic paraboloid failure surface criterion, which exemplifies the respective failure tensor polynomial. Introducing a stepwise form of loading of the specimens, we derive enough data for the accurate determination of these failure surfaces inside the elastoplastic region of loading, up to a complete failure. This parameter identification method was realized in an appropriate neural network environment via supervised and unsupervised learning algorithms. The network is trained to interpolate or extrapolate the existing experimental results, concentrated in all the compression quadrant of the principal stress-plane, to the entirety of the failure locus. Depending on the quantity of the experimental values and their reliability, the speed of convergence of the numerical method may be considered as satisfactory, yielding stable results after a few cycles of iteration.

* Π. Σ. ΘΕΟΧΑΡΗ, **Μελέτη τῆς Πολυαξονικῆς Ἀντοχῆς τοῦ Πολυκρυσταλλικοῦ Πάγου (Τύπου Ι).**

The method sketched was applied to a series of compression compression tests with ice I specimens for three successive steps of loading, corresponding either to the elastic limit of the material, or at the initial yielding, creating a volumetric conventional strain $\varepsilon_c = -0.2\%$, or at the peak strength of the material. Interesting results concerning the strength and the mode of fracture of this important material have been derived.

INTRODUCTION

Ice is a remarkably brittle solid compared to other materials at high homologous temperatures. Up to now much work has mainly developed on the study of creep and plasticity of ice, since these processes are known to dominate in ice sheets under small deviatoric stresses. However, ice fracture is also significant in many different aspects of the mechanical behavior of ice, especially in brittle fractures. Despite the importance of this mode of failure, less experimental work is devoted and no satisfactory fracture criteria for multiaxial loading of ice actually exist.

Since brittle fracture and cleavage are strongly influenced by the hydrostatic confinement of the ice, it is of paramount importance to establish a multiaxial criterion of fracture describing all the aspects of failure of this material. Then, a systematic experimental investifation of the failure modes under complex states of stress seem to be indispensable for defining the mode of resistance of such an important material. Polyaxial stress loadings along the principal directions of the substance have been sparcely executed for defining the failure mode of various types of ice.

Hausler (1981), as well as Schulson, Jones and Kuehn (1991) studied ice under multiaxial compressive stress and established the effect of confinement on the compressive mode of failure under brittle conditions. Furthermore, Rist and Murrell (1994) have undertaken tests under a triaxial mode of loading of polycrystalline ice I under compressive conditions, favourable to brittle fracture and microcracking. The influence of moderate confining lateral pressures was studied and it was shown that for low confining pressures brittle strength was strongly dependent on pressure. However, at higher confining pressures brittle strength was strongly dependent on pressure. However, at higher confinement, corresponding to a lateral compressive hydrostatic pressure equal to $\sigma_1 = \sigma_2 \geqslant 0.15\ \sigma_3$, fracture is resembling an overall shear type, where an oblique crack is established, followed eventually by wing sec-

ondary cracks, which are deceloped for lower than the above limit ratios of the lateral to the axial fracture stresses. This type of cracking of the specimen follows a sliding-wing mechanism of brittle fracture under overall compression.

It was further shown an all compressive triaxial testing, where a uniaxial stress is combined with a hydrostatic lateral pressure, was a sure means to promote a uniform stress field inside small specimens and therefore it was convenient to study the failure mode of such materials. For this purpose a conventional triaxial loading cell was used to study the mechanical behavior at low temperatures, corresponding to situations where ice of type I is formed and maintained during loading.

During the triaxial tests executed on cylindrical ice specimens an all compressive state of stress is applied to specimens, where the absolutely higher compressive stress σ_3 was directed along the axis of the cylindrical specimen, superposed by a lateral compressive stress state, where $\sigma_1 = \sigma_2 < \sigma_3$. By varying the combinations of such stress states, where the ratio $R = \sigma_3/\sigma_1$ was kept either below or slightly above the transition limit $R = 0.2$ different modes of fracture were obtained.

The definition of the yield stresses and loci for the various steps of loading considers a learning process of an appropriately defined numerical procedure using the least squares method with constrained conditions and based on the validity of the failure tensor polynomial working as a constitutive condition for progressive yielding. Then, the method consists in the construction of a numerical procedure, trained to fit existing experimental results, and to extend these results, which are normally obtained all in the compression octant, in the principal stress space, to the whole stress space. Having totally defined some intermittent particular yield loci of the material, based on a sufficient number of experimental points, it is possible to determine further subsequent yield loci to the existing already experimental yield surfaces, by considering the material as a *progressively changing anisotropic one*, whose variation of anisotropy is due to a further development of plasticity of the initial plastic enclaves (Theocaris and Panagiotopoulos (1995a)). The procedure is then instructed to *learn* the law of variation of anisotropy of the material, and, when it is applied to another set of experimental data, may fulfil its task to define the next step in shorter times and with higher accuracy. The method, making use of the flexibility of the failure tensor polynomial criterion, expressed by an elliptic paraboloid failure surface (EPFS), can establish the equi-

valent elastic failure characteristics, by using a continuously variable form of the EPFS. The details of the theory of the methods is fully presented in Theocaris and Panagiotopoulos (1995a, 1995b).

The crystal structure of ice may be described by a unit crystal which is extended indefinitely in all directions where each oxygen atom of the crystal is situated at the center of gravity of four neigbouring equidistant oxygen atoms, from each of which it is separated by hydrogen atoms, so that each hydrogen atom touches two neighbouring hydrogen atoms and each oxygen atom touches four hydrogens. according to the pattern of Fig. 1a. The three atoms do not lie in a straight line, but rather with the hydrogen atoms bent toward each other, so that the 3D-structure of the water molecule is unsymmetrical and can contain four uneven arms, placed inside a not-quite perfect cube. Thus, the angles formed by the two hydrogens and the respective central oxygen atom form angles equal about 105° and the distance between the oxygen and each hydrogen nucleus is equal to 0.96 A°. Opposite the hydrogen

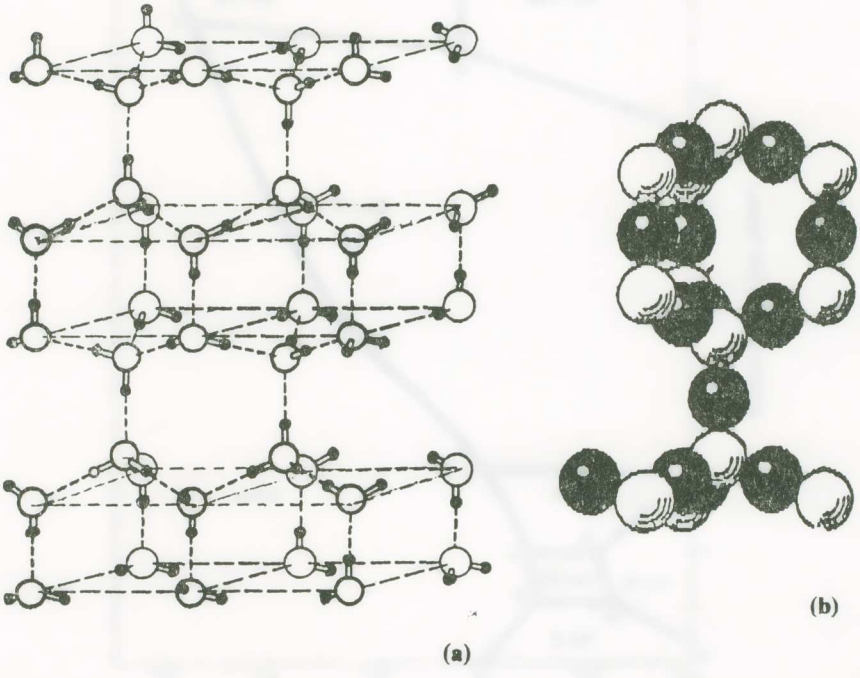

Fig. 1a. The atomic structure of the Ice (large circles correspond to oxygen atoms, small circles to hydrogen, long lines mean hydrogen bonds, while short lines correspond to covalent bonds). Fig. 1b. The tetrahedral arrangement of the water molecules.

atoms, and directed to the opposite corners of the unit cube, are formed two electronic clouds, which are the keys to the peculiar behavior of water, because they attract the hydrogen nucleus of an adjacent molecule of water, thus forming a hydrogen cloud (see Fig. 1b).

It has been established that a variety of structures are formed when water freezes, and they are identified by roman numerals. The structure represented in Fig. 1 corresponds to ice I, the familiar ice that forms, and it is stable, at ordinary atmospheric pressures. Nine different forms of ice are known, each definable by its lattice structure. Changes in temperature and pressure transform one kind of ice into another. The changes are specific and have been charted in phase diagrams (see Fig. 2). Thus, ice I at -10°C is converted under

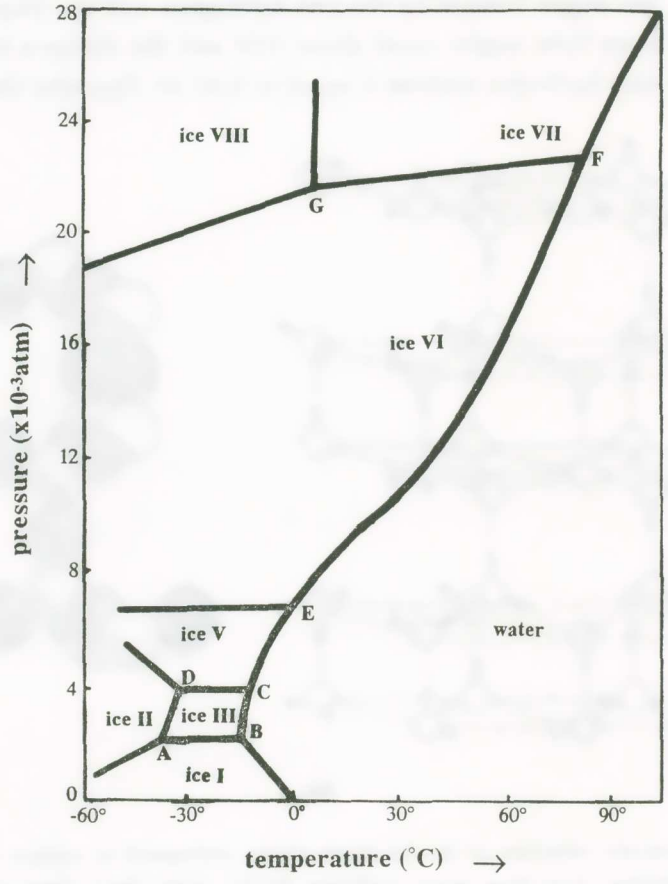

Fig. 2. The phase diagram of water at different temperatures and pressures.

a pressure of 4,400 atm to ice V, while at the same temperature level and under a pressure of 6,300 atm is converted to ice VI. Similarly, ice I at -30°C is converted to ice III at 2,200 atm, whereas, if the pressure is raised to 3,000 atm is converted to ice II. Furthermore, ice at -30°C is converted further to ice V and ice VI at higher pressures than 3,000 atm. Figure 2 presents a diagram of ice formation in terms of combinations of temperatures and pressures during its process of formation, where the equilibrium states are indicated for high - pressure forms of ice.

The present work focuses on the study of the mode of yielding and failing of polycrystalline ice close to the ductile brittle transition. Triaxial all compression tests were performed on fresh-water isotropic granular ice at a constant strain rate. We investigated the effect of triaxiality of the applied external loads on the mode of yielding and failing of this material. Since this material behaved as a quasi-brittle material the elliptic paraboloid failure surface criterion of failure for orthotropic materials was applied and interesting results and conclusions were derived concerning the mode of failure of this material up to failure under a triaxial mode of loading.

2. TRIAXIAL TESTING SYSTEM

A series of compression-compression tests were conducted on specimen of pure isotropic granular ice using a typical low temperature triaxial loading cell. The loading system utilizes clear silicone oil to impose hydrostatic confining pressure up to 20 MPa. Simultaneously, an axial load is applied to the specimens through a piston. The specimen was either cylindrical or rectangular. A compressive stress σ_3 was applied axially to the specimen under a confining pressure $p = \sigma_1 = \sigma_2$. The test temperature was maintained nominally to -20°C by adjusting the temperature of the cold room where the cell was contained with an adequate stability.

A systematic investigation of the mechanical behaviour of ice under triaxial testing requires cylindrical fine-grained specimens which should approach isotropy being consistent and of a reproducible quality. Thus, high density specimens of uniform size and with randomly oriented grains are necessary to be prepared. Therefore ice samples were prepared by flooding vaccumed moulds with sieved ice seeds with de-aerated water to achieve randomly oriented grained ice of uniform size of the order of five millimeter

in diameter. The specimens, which were all cylindrical, had dimensions of 40 mm in diameter and 100 mm in length. Constant strain rates were maintained during loading of the specimens in the loading direction, while lateral strains perpendicuîar to the loading direction were measured via two transducers of gauge length of 30 mm. Thus strains were measured in the central portions of the specimens. The main characteristics of the testing device are, therefore, a uniformly distributed and independently controlled device of application of a triaxial type of principal stresses, complemented by a system of accurate and rapidly measured strains in a large range of deformations, whereas the machine is a robust one, which disposes a high capacity of sustaining stresses of the order of 250 MPa.

For establishing the strength behaviour of three series of ice specimens under a triaxial mode of loading, and at a temperature of -20°C, a series of tests were conducted along loading paths following either the hydrostatic axis in the stress space, or paths with varying $\sigma_2 = \sigma_3$ stresses, while the σ_1 - principal stress was kept constant, or path in which the σ_1-and σ_2-stresses are kept constant at various levels and increased the σ_3-stress up-to-yielding and ultimate strength of the material.

Table 1 and Figure 3 present the strength data and the curves of variation of yield limits during triaxial loadings from the three successive series of all compressive tests at different strain rates, $\dot{e}$, varying between $\dot{e} = 10^{-2}$ to $\dot{e} = -10^{-4}$. All these strength data will be used for establishing the failure loci of ice, by applying the method propounded in this paper, and checking its efficiency and degree of reliability. The problem posed for the general anisotropic elastoplasticity law with respect to a given body may be expressed as follows: «Determine an anisotropic piecewise linear elasticity sequence of laws, for which a body with the same geometry, the same loading and the same constraints, exhibits a behaviour identical with the behaviour of the elastoplastic anisotropic body under study». If the loading function $p^{(t)}$ of the step $t \in [O, T]$ is given, we may divide [O, T] into the time instants $t^{(1)}$, $t^{(2)}$, ..., $t^{(n)}$ and denote by $C^{(1)}$, $C^{(2)}$, ..., $C^{(n)}$ the corresponding, but as yet unknown, anisotropic elasticity tensors, satisfying the well-known symmetry and ellipticity conditions. We seek $\{t^{(\rho)}, C^{(\rho)}\}$, $\rho = 1,...,n$, such that the solution of the anisotropic elasticity problem approximates as close as possible the solution of the initial anisotropic elastoplasticity problem. The problem is formulated as a parameter identification problem, where $z^{(\rho)} = \{t^{(\rho)}, C^{(\rho)}\}$,

are the control parameters and the strain, -stress, - and diplacement- fields are the state functions. The control parameters will be calculated by taking into account the experimental results as observation conditions. Assuming

TABLE 1

Summary of test results at different strain rates

Test Series No	Confining Compression stresses $\sigma_1 = \sigma_2$	Failure axial σ_3 = stress	Strain rate	Mode of Deformation
	MPa	MPa	s^{-1}	
	0.00	−2.20		Brittle
	0.12	18.10		Shear fracture
	1.30	22.24		Shear fracture
	2.41	26.79		
I	4.82	30.64		Ductile with
t = -20° C	10.30	43.72	$\dot{e} = 10^{-2}$	dense cracking
	19.80	54.40		
	28.50	60.91		Ductile
	30.00	62.82		
	0.00	−2.40		Ductile
	0.10	14.30		
	0.82	16.10		
II	4.61	22.48		Ductile with
t = -20¹ C	5.64	24.30	$\dot{e} = 10^{-3}$	dense cracking
	10.30	28.78		
	11.10	29.52		
	19.92	40.30		Medium
	29.74	49.91		cracking
	0.00	−1.85		Ductile with
	0.11	6.62		dense cracking
	4.70	15.21		
III	9.80	21.74	$\dot{e} = -10^{-4}$	Medium cracking
t = −20° C	19.88	32.12		
	28.80	40.78		Sparce

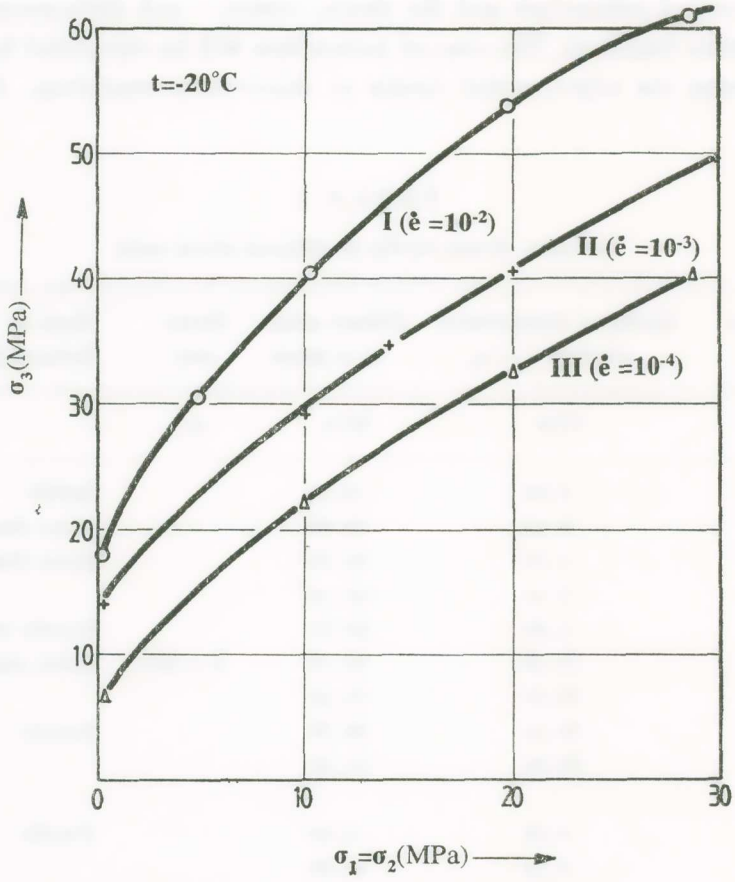

Fig. 3. Yield limits at the ultimate strength of ice in the (σ_3, $\sigma_2 = \sigma_1$)-space.

steps of small deformations, we denote by A_1, A_2 and A_3 the following differences:

$$A_1 = \sum_{\rho=1}^{n} \int_{\Omega} \left[u_{pl}^{(\rho)} - u_{el}^{(\rho)} \right]^2 d\Omega, \quad A_2 = \sum_{\rho=1}^{n} \int_{\Omega} \left[\varepsilon_{pl}^{(\rho)} - \varepsilon_{el}^{(\rho)} \right]^2 d\Omega,$$
$$A_3 = \sum_{\rho=1}^{n} \int_{\Omega} \left[\sigma_{pl}^{(\rho)} - \sigma_{el}^{(\rho)} \right]^2 d\Omega \qquad (1)$$

where u, ε and σ are respectively the displacements, strains and stresses, Ω is the body under consideration and the subcripts «el» and «pl» denote elastic or plastic quantities respectively.

The problem reads: Find $z^{(\rho)} = \{t^{(\rho)}, C^{(\rho)}\}$, $\rho = 1, ..., n$, such as to satisfy:

$$A_1 + A_2 + A_3 \to \min \tag{2}$$

where for every ρ, the quantities $\sigma_{el}{}^{(\rho)}$, $\varepsilon_{el}{}^{(\rho)}$ and $u_{el}{}^{(\rho)}$ satisfy the equations of equilibrium, the strain-displacement relations and the material law:

$$\varepsilon_{el}^{(\rho)} = C^{(\rho)}\, \sigma_{el}^{(\rho)} \tag{3}$$

The quantities $\varepsilon_{pl}{}^{(\rho)}$, $\sigma_{pl}{}^{(\rho)}$, $u_{pl}{}^{(\rho)}$, must satisfy the equilibrium equations, the compatibility conditions, and must agree with the experimental results concerning the relations between $\varepsilon_{pl}{}^{(\rho)}$ and $\sigma_{pl}{}^{(\rho)}$. Moreover, the quantities for both the initial plastic and elastic problems must satisfy the boundary conditions and the initial conditions at step $t = 0$. In the case of problems of elastoplasticity, where the A_1-condition, expressed by the first relation (1), may be ignored in the process and only as a checking condition of compatibility may be used, the arising parameter identifiction problem is of a non-classical nature and, therefore, it cannot be effectively treated by classical optimization methods. If we simplify the problems by discarding the A_1-condition and impose the discretized form of the elastic body to minimize the $(A_2 + A_3)$-deviation the resulting condition takes the form:

$$\sum_{\rho=1}^{n} \left[\sum_{r=1}^{m} \left(\left| \left| \varepsilon_{pl}^{(\rho)(r)} - \varepsilon_{el}^{(\rho)(r)} \left(z^{(\rho)} \right) \right| \right|^2 + \left| \left| \sigma_{pl}^{(\rho)(r)} - \sigma_{el}^{(\rho)(r)} \left(z^{(\rho)} \right) \right| \right|^2 \right) \right] \to \min \tag{4}$$

$$K\left(z^{(\rho)}\right) u^{(\rho)} + p^{(\rho)} = 0 \tag{5}$$

where $r = 1,..., m$ enumerates the discrete degrees of freedom, $K(.)$ is the elasticity stiffness matrix and the symbol $I\ .\ I$ denotes the corresponding Euclidean norms. The stiffness matrix K corresponds to the geometry of the body, whose quantities $\sigma_{pl}{}^{(\rho)}$ and $\varepsilon_{pl}{}^{(\rho)}$ are defined experimentally at the step intervals $t^{(\rho)}$. Finally, $p^{(\rho)}$ is the loading function, which leads to the experimental results at the ρ-step.

Relation (4) can be replaced by (Theocaris & Panagiotopoulos, (1995)):

$$\max_{\rho,r} \left\{ \left| \left| \varepsilon_{pl}^{(\rho)(r)} - \varepsilon_{el}^{(\rho)(r)}\, z^{(\rho)} \right| \right| + \left| \left| \sigma_{pl}^{(\rho)(r)} - \sigma_{el}^{(\rho)(r)}\, z^{(\rho)} \right| \right| \right\} \to \min \tag{6}$$

or, by the prescribed error inequalities:

$$\max_{p,r,i,j} \left| \varepsilon_{plij}^{(\rho)(r)} - \varepsilon_{elij}^{(\rho)(r)}(z^{(\rho)}) \right| \leq \delta, \ \max_{p,r,i,j} \left| \sigma_{plij}^{(\rho)(r)} - \sigma_{elij}^{(\rho)(r)}(z^{(\rho)}) \right| \leq \delta, \qquad (7)$$

The inequalities (7) imply that the maximum differences between the elastic and the plastic stress-and strain-components respectively at any point of the body, and at any control moment $t^{(\rho)}$, cannot be larger than a given constant δ. For a given sequence of strains, even in different directions, we can assume that z includes only the anisotropic elasticity moduli $C^{(\rho)}$, where we assign at each loading step several control parameters, $C^{(\rho_1)}$, $C^{(\rho_2)}$, ..., $C^{(\rho_\nu)}$, in order to approximate, in a reliable manner, the anisotropic plasticity stress -and strain- fields.

In this way the parameter identification problem is an inverse problem in structural analysis, where a solution is prescribed and we ask for convenient elastic properties and/or loading and/or geometric quantities, producing a solution very close, or identical, to the prescribed one. Obviously, we have to solve a minimum deviation problem having as subsidiary conditions all the relations characterizing the solution. Indeed, in adapting the structural analysis to the numerical approximation computation it is necessary to formulate the structural analysis problem as a minimization problem and the same procedure is used for the parameter identification problem described by relations (4) and (5) where a quadratic deviation function should be minimized. Then, we have to solve the linear system (5) corresponding to a linear elastic structure for each value of the control vector $z^{(\rho)}$.

If now the components of strains and stresses, $\varepsilon_{el}{}^{(\rho)}$ and $\sigma_{el}{}^{(\rho)}$, corresponding to the displacements $u_{el}{}^{(\rho)}$, are prescribed, or they must take values very close to respective $\varepsilon_{pl}{}^{(\rho)}$-, $\sigma_{pl}{}^{(\rho)}$-values, for all stresses and strains of the structure under consideration, and for all ρ we need to determine the control vectors $z^{(\rho)}$, $\rho = 1, ..., n$, i.e. to the corresponding control times $t^{(\rho)}$, as well as the elasticity coefficients $C^{(\rho)}$, such as to minimize the differences in (4) after an appropriate discretization of the structure. For each value of $z^{(\rho)}$, $\rho = 1, ..., n$, the structure will be calculated by means of the numerical procedure, introduced through Eqs. (6) and (7).

3. THE TENSOR POLYNOMIAL FAILURE CRITERION

Considering that ice should be an orthotropic brittle material we have to define the failure tensors H_{ij} and h_i along the principal stress axes, where i, j = 1, ..., 3 and the 3-axis is taken to be the strong axis of the medium. We assume further that the principal stress axes coincide with the material principal strength axes. In this case, the failure surface is expressed by (Theocaris, 1987a,c):

$$H_{11}(\sigma_1^2+\sigma_2^2)+H_{33}\sigma_3^2-(2H_{11}-H_{33})\sigma_1\sigma_2-H_{33}(\sigma_2\sigma_3+\sigma_3\sigma_1)+h_1(\sigma_1+\sigma_2)+h_3\sigma_3=1 \quad (8)$$

The quadric surface (8) is an elliptic paraboloid surface, whose axis of symmetry is parallel to the hydrostatic axis $\sigma_1=\sigma_2=\sigma_3$ and it is symmetric to the principal diagonal plane (σ_3,δ_{12}), containing the σ_3-axis and passing through the bisector δ_{12} of the angle $\sigma_1 0\sigma_2$.

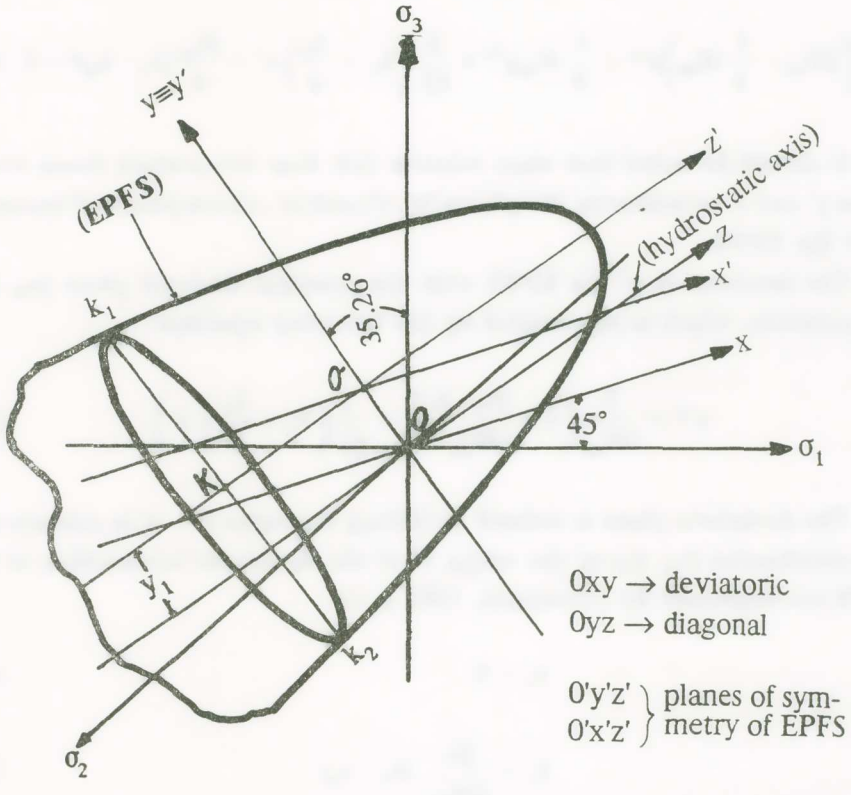

Fig. 4. The elliptic paraboloid failure surface (EPFS) for the transversely isotropic body.

Figure 4 exhibits the elliptic paraboloid failure surface whose axis of symmetry K0′z′ is parallel to the 0z-hydrostatic axis, in the principal stress space $(\sigma_1, \sigma_2, \sigma_3)$. The Cartesian reference system Oxyz is formed by rotation of the $(\sigma_1, \sigma_2, \sigma_3)$-system, so that the 0x-axis becomes a bisector of the (σ_1, σ_2)-plane, the 0z-axis coincides with the hydrostatic axis, and the 0y-axis forms a tri - orthogonal system. In addition, the 0x′y′z′-system is formed from the 0xyz - system by translating the origin 0 to the new origin 0′ by a distance y_1.

The distance y_1 between the hydrostatic axis and the axis of symmetry of the EPFS is given by:

$$y_1 = \frac{\sqrt{6}}{9H_{33}} (h_1 - h_3) \tag{9}$$

Relation (8) when referred to the Cartesian coordinate system 0x′y′z′ becomes (Theocaris, 1987 a,c):

$$\left(2H_{11} - \frac{1}{2} H_{33}\right)x'^2 + \frac{3}{2} H_{33}y'^2 + \frac{2}{\sqrt{3}}\left(h_1 + \frac{h_3}{2}\right)z' + \frac{H_{33}}{9}(h_1 - h_3)^2 = 1 \tag{10}$$

It should be noted that since relation (10) does not contain linear terms in the y′ and x′ coordinates, the planes (y′, z′) and (x′, z′) are planes of symmetry of the EPFS.

The intersection of the EPFS with the principal diagonal plane (σ_3, δ_{12}) is a parabola, which is represented by the following equation:

$$y'^2 = \frac{2}{3H_{33}}\left(1 + \frac{(h_1 - h_3)^2}{9H_{33}^2} + \frac{2}{\sqrt{3}}\left(h_1 + \frac{h_3}{2}\right)z'\right) \tag{11}$$

The deviatoric plane is defined by letting the value $z' = 0$ in relation (9). The coordinates (x_1, y_1) of the origin 0′ of the deviatoric intersection of the EPFS are expressed by (Theocaris, 1987 a, c):

$$x_1 = 0 \tag{12}$$

$$y_1 = \frac{\sqrt{6}}{9H_{33}} (h_1 - h_3) \tag{13}$$

Finally, the distances d and d′ between the deviatoric π-plane and either the point of piercing of the hydrostatic axis z, or the axis of symmetry of the EPFS z′ are expressed by:

$$d = -\frac{\sqrt{3}}{2\left(h_1 + \frac{h_3}{2}\right)} \tag{14}$$

$$d' = \frac{\sqrt{3}}{2\left(h_1 + \frac{h_3}{2}\right)}\left(1 + \frac{(h_1 - h_3)^2}{9H_{33}}\right) \tag{15}$$

Because of the symmetry of the EPFS with respect to the principal diagonal plane (σ_3, δ_{12}), the intersections of this surface with either principal stress plane (σ_1, σ_3) or (σ_2, σ_3) are identical. Therefore, only one needs to be studied. The cross-section of the EPFS by the principal plane (σ_1, σ_2) may be derived from relation (8) by setting $\sigma_2 = 0$. This substitution yields:

$$H_{11}\sigma_1^2 + H_{33}\sigma_3^2 + 2H_{31}\sigma_3\sigma_1 + h_1\sigma_1 + h_3\sigma_3 = 1 \tag{16}$$

Relation (16) under the condition of its discriminant to be positive (for $4H_{33} > H_{11}$) is an ellipse (see Fig. 5). The center of this ellipse has coordinates (σ_{3M}, σ_{1M}). These coordinates together with the angle λ_{13} of inclination of the polar radius (OM) are given by (Theocaris, 1988b):

$$\sigma_{1M} = \left(\frac{2h_1 H_{33}^2 + h_3 H_{11}^2}{4h_3 H_{11} - h_1 H_{33}}\right) \tag{17}$$

$$\sigma_{3M} = \left(\frac{h_1 H_{33} + 2h_3 H_{11}}{H_{33}(4H_{11} - H_{33})}\right) \tag{18}$$

$$\lambda_{13} = \tan^{-1}\left[\frac{h_1 H_{33} + 2h_3 H_{11}}{H_{33}(2h_1 + h_3)}\right] \tag{19}$$

The system of Cartesian coordinates to which this ellipse is central and symmetric, is defined by the angle θ_{13}, expressed by:

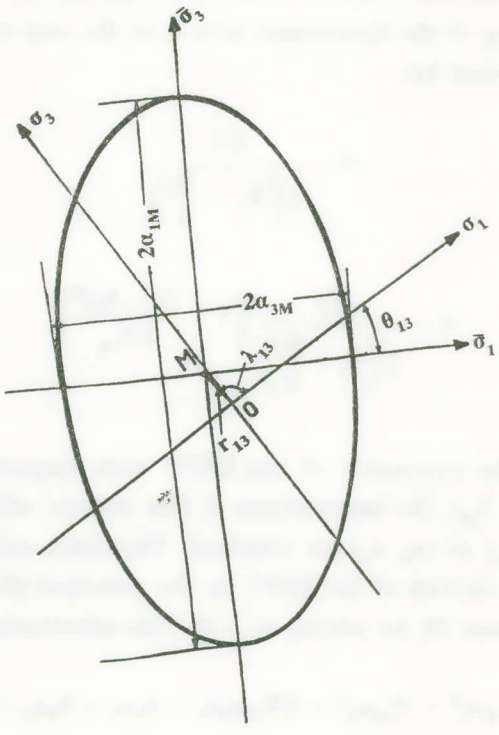

Fig. 5. The intersection of the EPFS by the (σ_3, σ_1)-principal stress plane.

$$\theta_{13} = 1/2\tan^{-1}\left[H_{33}/(H_{11} - H_{33})\right] \tag{20}$$

The lengths of the semi-axes a_{1M} and a_{3M} of the ellipse are given by:

$$(a_{1M}, a_{3M}) = \left(\frac{C}{\delta_{12}}\right)^{1/2} \tag{21}$$

where

$$C = -\frac{\det A_3}{\det A_2} = -\frac{\begin{vmatrix} H_{11} & H_{13} & \frac{h_1}{2} \\ H_{13} & H_{33} & \frac{h_3}{2} \\ \frac{h_1}{2} & \frac{h_3}{2} & -1 \end{vmatrix}}{\begin{vmatrix} H_{11} & H_{13} \\ H_{13} & H_{33} \end{vmatrix}} \tag{22}$$

and δ_{12} are the roots of the characteristic equation:

$$\delta^2 - \mathrm{tr}A_{ii}\delta + \det A_2 = 0 \qquad (23)$$

The above cited analysis completes the exact study of the form of the failure criterion by yielding sufficient information concerning the form, shape dimensions and orientation of the important intersections of the failure locus of the material under study and therefore describe accurately its failure mode under any triaxial loading path.

4. EXPERIMENTAL EVIDENCE OF TRIAXIAL TEST ON ICE

The experimental scheme described previously will now be applied for the study of the yield and failure loci of ice at different strain rates. As the basis of the calculations the numerical results included in Table 1 will be used for the definition of the failure loci under triaxial loading. We consider the experiments described in section 3 of this paper concerning the failure modes of a coarse grained dense crystalline material, whose strength differencial effect is predominant in its mode of failure. It is assumed that the stress data given in Tables 2 and 3 are the data for the parameter identification problem of the form (4) and (5), with the slight modification, that, in (4), only the stress difference terms exist and the strains are not taken into account. Moreover, we have followed the loading-unloading procedures, as described in the experiments and we have assumed as unknowns of the problem only the two - dimensional anisotropic elasticity coefficients. Thus, we can approximate the anisotropic hardening plasticity behaviour, including the stregth differential effect with, a variable linear elastic behaviour defined by the appropriate changing anisotropy.

The numerical procedure for the evaluation of the failure:

We consider as given the experimental yield points on the failure surfaces for subsequent loading steps inside the elastic-plastic region of loading and unloading of the specimens. On each given yield surface we take a finite number of points $\sigma_{ij} = (i = j = 1, 2, 3)$ and we apply with respect to all given yield surfaces the numerical procedure of the previous section. We assume that the elastic material is transversely isotropic, of changing anisotropy with loading, and we want to determine the sequence of the orthotropy coefficients $\alpha_{11}^{(\rho)}$,

$\alpha_{22}^{(\rho)}$, $\alpha_{12}^{(\rho)} = \alpha_{21}^{(\rho)}$, $\alpha_{33}^{(\rho)}$ within each element, which satisfy the identification problem for the stresses and constitute the elasticity tensor $C^{(\rho)}$ at the ρ-step of the learning algorithm. As $\rho \to \infty$ we have theoretically the solution tensor $C = \{\alpha_{11}, \alpha_{22}, \alpha_{12} = \alpha_{21}, \alpha_{33}\}$. We recall here that $\varepsilon_x = \alpha_{11}\sigma_x h + \alpha_{12}\sigma_y h$, ..., $\gamma_{xy} = \alpha_{33}\sigma_{xy} h$, where $h = 1mm$ is the thickness of the plane structure.

In order to get a more reliable approximation of the anisotropic elastoplastic problem with a sequence of anisotropic elastic problems, we have considered intermediate yield points through interpolation between two experimentally given failures in the 3D-stress space. The interpolation is guided by assuming that the respective loading step corresponds to a point at the surface of the elliptic paraboloid failure surface for the general anisotropic hardening elastoplastic body presenting the strength differential effect (Theocaris

TABLE 2

The values of the terms of the elliptic paraboloid failure surface, as well as the characteristic quantities defining the deviatoric and the principal (σ_3, δ_{12}) diagonal plane intersections of the EPFSs

Loading Series	H_{11}	H_{22}	H_{33}	h_1	h_2	h_3	Remarks
I ($\dot{e} = 10^{-2}s^{-1}$)	0.4542	0.4542	1.5139	12.993	12.993	0.0553	All Hij & hii
II ($\dot{e} = 10^{-3}s^{-1}$)	1.4123	1.4123	4.7078	0.0068	0.0068	21.1610	must be mult-
III ($\dot{e} = 10^{-4}s^{-1}$)	3.7261	3.7261	12.420	0.0037	0.0037	23.266	plied by ($x10^{-3}$)

	Deviatoric Plane					
	x_d	y_d	r_d	Ψ_d	$\alpha_{1/2}$	$\alpha_2/2$
I ($\dot{e} = 10^{-2}s^{-1}$)	0	2.335	2.335	90°	81.776	21.115
II ($\dot{e} = 10^{-3}s^{-1}$)	0	−1.223	−1.223	90°	46.331	11.963
III ($\dot{e} = 10^{-4}s^{-1}$)	0	−0.5098	−0.5098	90°	28.443	7.344

	(σ_3, δ_{12}) - diagonal plane ($z = \alpha y^2 + \beta y + \gamma$)					
	α	β	γ	δ_{12p}	σ_{3p}	η_3
I ($\dot{e} = 10^{-2}s^{-1}$)	0.1513	−0.7067	−66.6398	38.9496	51.0389	40.8572
II ($\dot{e} = 10^{-3}s^{-1}$)	0.5760	1.4141	−81.8447	46.2541	67.5321	46.2541
III ($\dot{e} = 10^{-4}s^{-1}$)	1.3869	1.4142	74.4419	42.5628	61.0754	42.7709

TABLE 3

The values of the characteristic quantities defining the (σ_1, σ_2), (σ_1, σ_3), and (σ_2, σ_3) principal stress intersections for the EPFSs

Loading Series	σ_{1M}	σ_{2M}	λ_{12}(**)	r_{12}	α_{1M}	α_{2M}	θ_{12}(**)
			Principal Stress Plane (σ_1, σ_2)*				
I ($\dot{e} = 10^{-2}s^{-1}$)	−8.5826	−8.5826	45°	12.1376	85.6869	38.3203	45°
II ($\dot{e} = 10^{-3}s^{-1}$)	−0.001	−0.001	45°	0.002	46.0883	20.6113	45°
III ($\dot{e} = 10^{-4}s^{-1}$)	0	0	45°	0	28.3748	12.6896	45°
			Principal Stress Plane (σ^1, σ^3)*				
	σ_{M1}	σ_{3M}	λ_{13}(**)	r_{13}	α_{1M}	α_{3M}	θ_{13}(**)
I ($\dot{e} = 10^{-2}s^{-1}$)	−42.9240	−85.8443	26.57°	95.9776	161.0533	28.5740	27.50°
II ($\dot{e} = 10^{-3}s^{-1}$)	−13.4855	−22.4762	30.96°	26.2114	78.2191	13.8776	27.50°
III ($\dot{e} = 10^{-4}s^{-1}$)	−5.6199	−9.3665	30.96°	10.9231	46.4987	8.2498	27.50°

* All stresses in MPa's.

** Negative angles are measured from the negative principal axes with the lower index.

(1989 a,b)). The failure surface in any principal stress plane is an ellipse, which can be defined by a series of adequate points. The same property is valid for the deviatoric plane, as well as for any intersection parallel to this plane. The only exception to the general rule holding for the EPFS-criterion is for intersections of the failure paraboloid by planes containing the hydrostatic axis or the axis of symmetry of the paraboloid. These intersections are all parabolas (Theocaris, (1989a) (1989b)). After the initial rough guess of a number of basic yield surfaces derived from a series of different experimentally determined triads of values of the principal stresses, leading to different points of presumably the same yield surface, we obtain a family of different failure loci corresponding to equivalent loading steps, but of different loading paths in the three dimensional principal stress space, which describe in a convenient way the failure mode of the material in multiaxial loading.

Applying the above described method to the three series of experimental results from the series of tests with ice cylinders at different strain rates we

evaluated the corresponding EPFS loci to the respective values for each triad of σ_1, σ_2 and σ_3 given in Table 1. It was assumed in this analysis that the instantaneous values of the failure and strength differential effect tensors H_{ij} and h_i, as derived from the least square approximation scheme, belong to a certain failure surface of an equivalent transversely isotropic elastic body with values of H_{ij} and h_i those considered and this failure surface is progressively changing satisfying always the respective, experimentally obtained, values for the principal stresses. However, one should notice that the calculated orthotropic elasticity coefficients are fictitious and they have generally nothing in common with the elasticity coefficients of the elastoplastic material. Moreover, they are not uniquely determined. Furthermore, the larger is the number of unknowns to be determined, the less accurate is the method. In order to check the stability and accuracy of the numerical procedure we have to define the limits of the constraint H_{bound} satisfying the inequality derived from the so-called «*stability conditions*» expressed by (Theocaris, (1989b)):

$$H_{ii}H_{jj} - H_{ij}^2 > H_{bound} \geqslant 0$$

The numerical procedure of defining the failure hyperspace was based on different combinations of experimental data. The limits for the H_{bound} were taken to vary between 1×10^{-9} and 1×10^{-11}, so that a high accuracy can be obtained. Thus, the sets of hypersurfaces, derived from these combinations, created coherent entities of curves with insignificant deviations between them, thus indicating the stability of the method. Only when some of the initial values were selected at the borders of each loading zone, where either elacticity was in doubt, or the strain rates were rapidly changing, some scattering of these zones appeared in the plottings, which indicated the high sensitivity of the method.

The three distinctive series of tests of Ice I tested gave finally the following values of the terms of the respective tensors H_{ij} and h_i contained in Table 1. In the same table the values of the pairs of principal stresses in tension and compression σ_{Ti} and σ_{Ci} for the three loading steps are also tabulated. Having at our disposition these values of stresses and of the coefficients H_{ij} and h_i we can readily define the various intersections of the failure hyperspaces.

a) The deviatoric plane of the EPFS's:

The center of this intersection, as well as the polar distance r_d and the angle ψ_d subtended by this polar distance and the 0''x''-axis of the paraboloid are given by relations (12) and (13) and they yield:

$$r_d = y_1 = \frac{\sqrt{6}}{9H_{33}} (h_1 - h_3)$$

and $$\psi_d = 0^o$$

Indeed, since the material is a transversely isotropic one, the orientation and the size of the intersection of the failure surface by the deviatoric plane, which is an ellipse, has its center along the axis of symmetry of the paraboloid and its principal axes are parallel to the 0'x' anc 0'y'-axes of the yield surface.

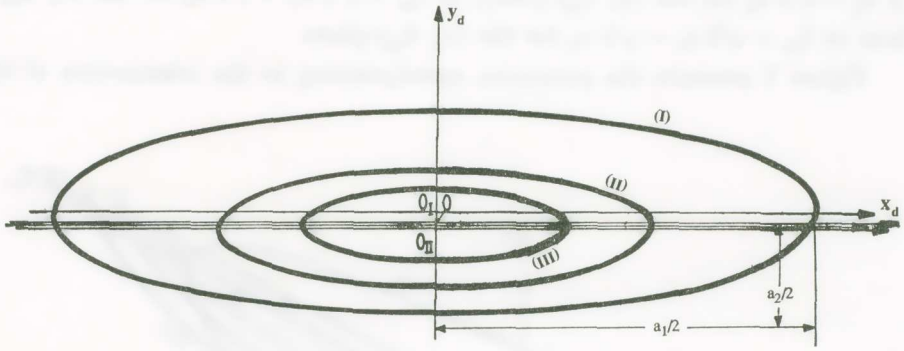

Fig. 6. The deviatoric plane failure intersections of the EPFS for ice I at different strain rates.

Figure 6 present the elliptic intersection of the failure hypersurface by the deviatoric π-plane and Table 1 the coordinates of the centers of the three ellipses corresponding to the three series of tests with ice. Furthermore, the polar distance r_d and the inclination to the (–x)-axis of this radius, ψ_d, is given, as well as the lengths of the principal axes of the ellipses and their inclinations of the longest axis relatively to the (-x)-axis.

It is clear from Fig. 6, as well as from the table 2 that while the center 0_1 of the elliptic locus of the deviatoric plane for the first series of tests with ice

lies above the hydrostatic axis 0z ($y_1 > 0$) the two other centers of the ellipses for the series II and III of tests lie beneath this axis ($y_1 < 0$). The shapes of all three elliptic intersections of the deviatoric plane are horizontally oblong indicating that the material tested is strongly anisotropic along the transverse principal (σ_1,σ_2)-plane with the σ_3-stress axis the weakest of all three axes. Then, it may be concluded that ice I under the conditions of the present testing behaves like a weak-axis woven fabric composite, whose transverse plane behaves isotropically (Theocaris, (1992)).

b) The principal diagonal intersections of the elliptic paraboloid:

The intersections of the failure hyperspace by the three principal diagonal planes (σ_3, δ_{12}), (σ_1, δ_{23}) and (σ_2, δ_{13}) are all parabolas, whose axes of symmetry are parallel to the 0z-hydrostatic axis and lying at different distances from it. Their equations are derived from relation (8) by putting either $\delta_{12} = \sqrt{2}\ \sigma_1 = \sqrt{2}\ \sigma_2$ for the (σ_3, δ_{12})-plane, or $\delta_{23} = \sqrt{2}\ \sigma_2 = \sqrt{2}\ \sigma_3$ for the (σ_1, δ_{23})-plane or $\delta_{13} = \sqrt{2}\ \sigma_1 = \sqrt{2}\ \sigma_3$ for the (σ_2, δ_{13})-plane.

Figure 7 presents the parabolas corresponding to the intersection of the

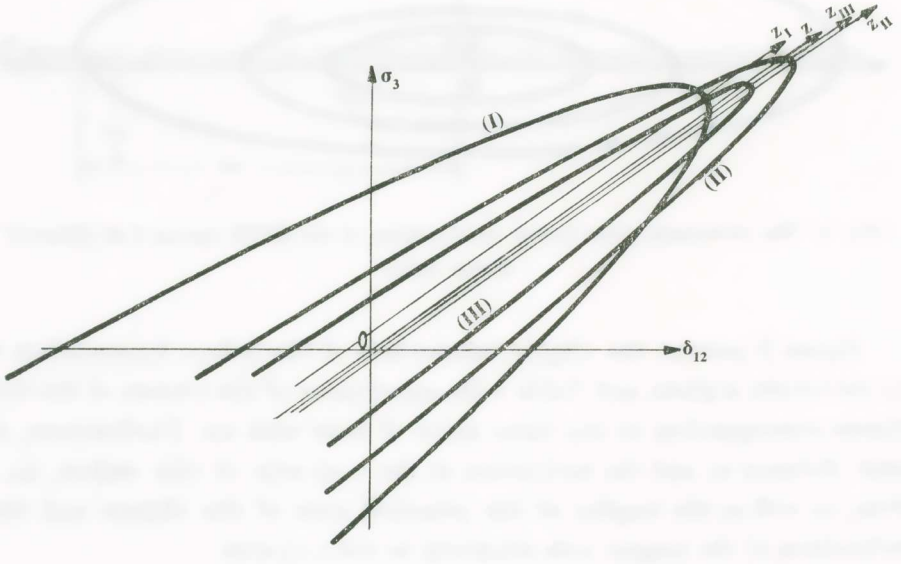

Fig. 7. The principal diagonal plane (σ_3, δ_{12})-intersections of the EPFS for ice I at different strain rates.

failure loci by the (σ_3, δ_{12})-principal diagonal plane. It is obvious from these plottings that, as the strain rate of loading of the material decreases, the elliptic paraboloids become more and more shallow, and the distances of their symmetry axes from the hydrostatic axis increase progressively. It has been already shown that, when the anisotropy of the material is increasing its representative failure locus becomes progressively shallower and the coordinates η and ξ of the distance between the symmetry axis of the paraboloid and the hydrostatic axis are also increasing (Theocaris, (1989a, b)). Then, it may be concluded that any increase of the strain rate of the loading of the ice results in a tendency of the material to behave as a less anisotropic material tending to become quasi-isotropic.

Table 2 gives the characteristic dimensions of the principal diagonal (σ_3, δ_{12})-plane, that is its equation with the coefficients α, β,γ, the coordinates of the vertex of the (σ_3, δ_{12})-parabola, as well as the distances η_i between its symmetry axis and the hydrostatic axis along the y-axis of the EPFS. It is worthwhile indicating again that the axes of symmetry of the three hyperbolas of

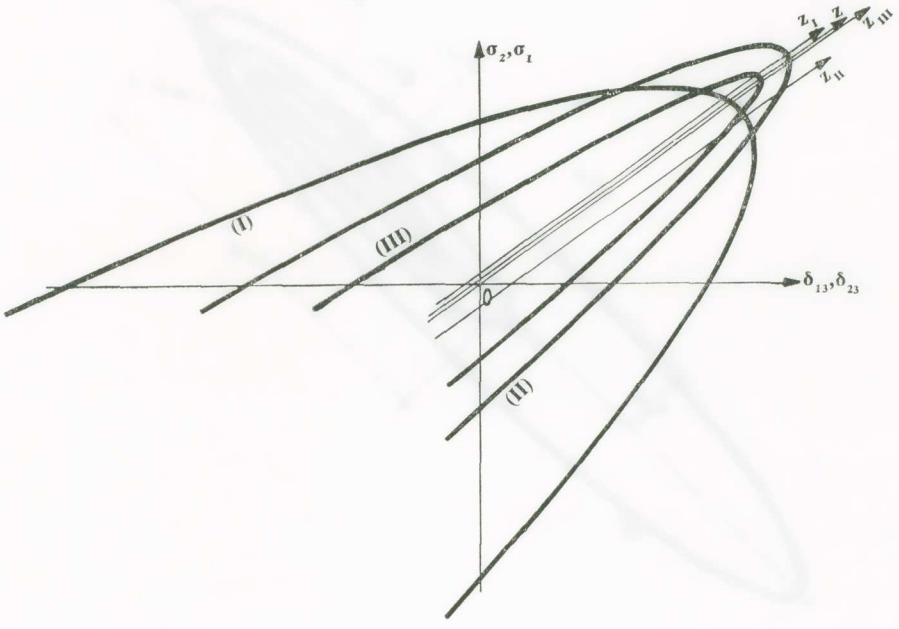

Fig. 8. The principal diagonal plane (σ_2, δ_{13}) and (σ_1, δ_{23})-intersections of the EPFS for ice I at different strain rates.

Fig. 7 representing the failure loci of the ice are placed on both sides of the hydrostatic axis with the loading step corresponding to the lower strain rate $\dot{e} = 10^{-2}s^{-1}$ lying above this axis, whereas the axes of the two remaining loading rate loadings lying beneath the hydrostatic axis.

Figure 8 presents the parabolas of intersections of the failure loci for the three series of tests by the planes (σ_2, δ_{13}) and (σ_1, δ_{23}) which are both groups of identical curves. However, since these intersections do not correspond to a symmetric section of the failure locus and therefore their axes of symmetry are relatively displaced when projected to the respective planes.

Again, it can be pointed out that the parabola corresponding to the loading step with the lower strain rate ($\dot{e} = 10^{-2}s^{-1}$) is the more shallower than the other two loci corresponding to higher strain rates. Again, the relative positions and sizes of these intersections indicate that the failure-surface of the material takes an oblate shape relatively to its transverse isotropic plane.

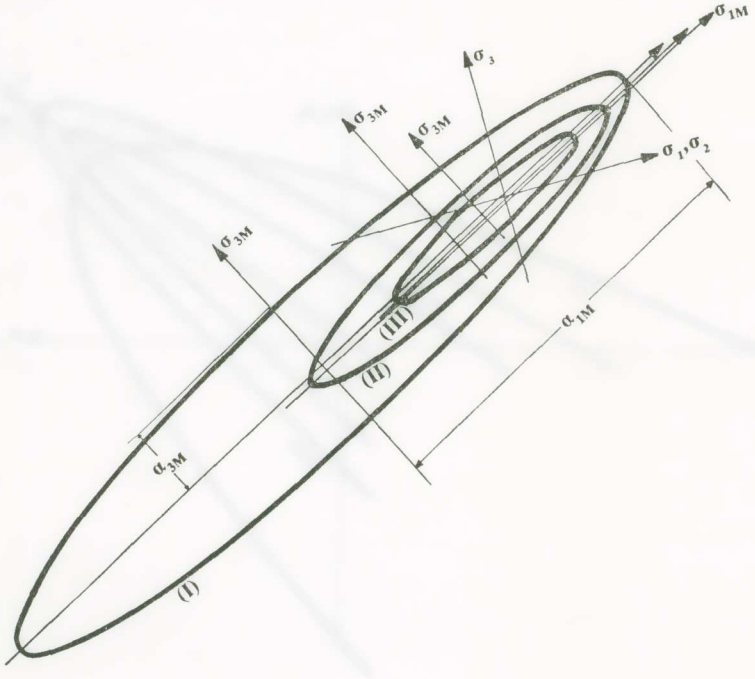

Fig. 9. The principal stress plane (σ_1, σ_3)-intersections of the EPFS for ice I at different strain rates.

c) The principal ($\sigma_i\sigma_j$)-stress intersections of the EPFS.

The equations expressing these intersections of the failure hypersurface by the principal stress planes are given by relations (16) to (23) where the explicit expression for the (σ_1, σ_2)-principal stress plane is given as well as the coordinates (σ_{1M} and σ_{3M}) of its center and the lengths α_{1M} and α_{3M} of its semi-axes. Similar relationships are valid for the two other principal stress planes (($\sigma_1\sigma_2$) and ($\sigma_2\sigma_3$)), where these equations are established by cyclic rotation of the indices. Table 3 contains all the necessary dimensions for plotting these intersections.

Figure 9 presents the intersections of the EPFS by the ($\sigma_1\sigma_3$)-principal

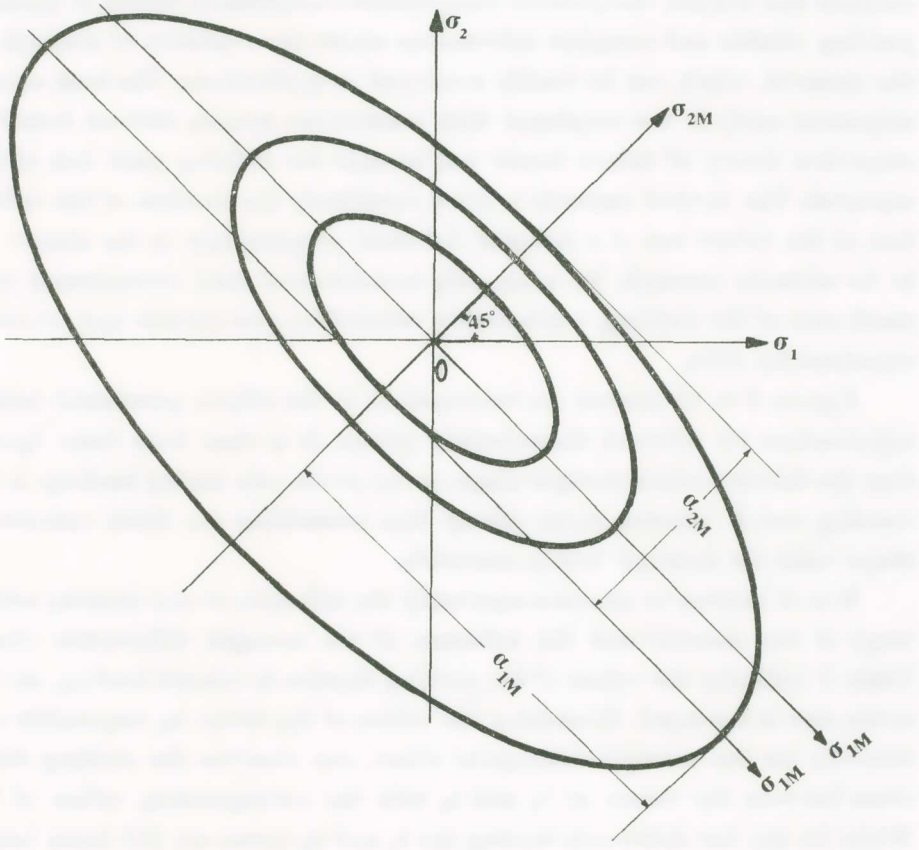

Fig. 10. The principal stress plane (σ_1, σ_2)-intersections of the EPFS for ice I at different strain rates.

stress plane for the three series of tests on ice, whereas Figure 10 gives the intersections of the EPFS by the isotropic stress-plane ($\sigma_1\sigma_3$). It is worthwhile indicating that these intersections are symmetric to axes subtending angles of 45 degrees with the principal stress axes and the elliptic intersections are oblate to the hydrostatic axis.

5. RESULTS

From the extensive analysis, based on the definition of failure surfaces for three series of tests in compression compression of specimens of ice I at different strain rates the evolution of the shape and form of the failure hypersurface of the material during loading was solidly established, by using only uniaxial and triaxial compression-compression-compression modes of loading, yielding reliable and complete information about the evolution of strength of the material, which can be readily employed in applications. The least square numerical analysis was employed with constrained bounds derived from the respective theory of failure tensor polynomials for defining yield loci of the materials. The method succeeds to solve completely the problem of the definition of the failure loci of a material deformed progressively in the elastic, up to its ultimate strength, by using only experimental data concentrated in a small area of the yielding, conveniently selected to give reliable and accurate experimental data.

Figures 6 to 10 present the intersections of the elliptic paraboloid failure hypersurface by different characteristic planes. It is clear from these figures that the failure surface changes shape as the strain rate during loadings is increasing and it becomes more oblong thus resembling the Mises cylindrical shape valid for isotropic brittle materials.

It is of interest to examine separately the influence of any existing anisotropy of the material and the influence of the strength differential effect. Table 3 indicates the values of the yielding stresses in triaxial loading, as the strain rate is increased. Examining the values of the terms h_i, responsible exclusively for the strength differential effect, one observes the striking difference between the values of h_1 and h_2 with the corresponding values of h_3. While for the low strain rate loading the h_1 and h_2-terms are 250 times larger than h_3, for the other two higher strain rates this relation is reversed with the h_3-term to be 3000 to 6000 times larger than h_1 and h_2. This difference between

the values of the tensor terms h_i together with a similar discrepancy between the orders of magnitude of the terms of the H_{ij}-tensor, where H_{33} is threefold and more larger than $H_{11} = H_{22}$, explains the higher lateral strength of ice appearing markedly in all the intersections of failure loci, fact which may be explained by the crystallic structure of ice under such environmental conditions.

ACKNOWLEDGEMENT

The reserach programme presented in this paper was supported by the National Academy of Athens research funds No 200/285. The author expresses his appreciation for this generous support. The author is indebted to his secretary Mrs. Anny Zografaki for helping him in typing the manuscript and plotting the figures of the paper.

REFERENCES

[1] F. U. Hausler, «Multiaxial Compressive Strength Tests on Saline Ice with Brush - Type Loading Platens», Proceedings in IAHR, Intern. Symp. on Ice, Quebec Can. Vol. II, (1981), 526-536.

[2] M. A. Rist and S. A. F. Murrell, «Ice Triaxial Deformation and Fracture», Journal of Glaciology, 40 (135), (1994), 305-318.

[3] E. M. Schulson, D. E. Jones and G. A. Kuehn, «The Effect of Confinement on the Brittle Compressive Fracture of Ice», Annals of Glaciology, 15, (1991), 216-221.

[4] P. S. Theocaris, «The Paraboloid Failure Surface for the general orthotropic material», Acta Mechanica, 79 (1), (1989a) 53-79.

[5] P. S. Theocaris, «The Elliptic Paraboloid Failure Surface for Transversely Isotropic Materials off-axis Loaded», Rheologica Acta, 28 (1989b) 154-165.

[6] P. S. Theocaris, «Failure Criteria for Anisotropic Bodies», Handbook of Fatigue Crack Propagation in Metallic Structures, A. Carpinteri Editor, Elsevier, Amsterdam, Publ., 1, (1994) 3-45.

[7] P. S. Theocaris and P. D. Panagiotopoulos, «Plastocity Including the Bauschinger effect Studied by a Neural Network Approach», Acta Mechanica, 113, No. 1-4, (1995a), 63-75.

[8] P. S. Theocaris and P. D. Panagiotopoulos, «Generalized Hardening Plasticity Approximated via Anisotropic Elasticity: A Neural Network Approach», Computer Methods in Appl. Mech. and Engng., 125 (2), (1995b), 123-139.

ΠΕΡΙΛΗΨΙΣ

Μελέτη τῆς Πολυαξονικῆς Ἀντοχῆς τοῦ Πολυκρυσταλλικοῦ Πάγου (Τύπου Ι)

Εἰς τὴν παροῦσαν ἐργασίαν, ἐπιχειρεῖται πειραματικὴ μελέτη διὰ τὸν προσδιορισμὸν τῶν κριτηρίων ἀστοχίας τοῦ πολυκρυσταλλικοῦ κοκκώδους πάγου εἰς θερμοκρασίας περὶ τοὺς -20° C. Διὰ τὸν προσδιορισμὸν τῆς ἐπιφανείας ἀστοχίας τοῦ ὑλικοῦ αὐτοῦ ἐχρησιμοποιήθησαν ὡς δεδομένα σειρὰ τριαξονικῶν θλιπτικῶν καταπονήσεων, μὲ τὰς δευτερευούσας παραπλεύρους τάσεις σ_1 καὶ σ_2 ἴσας μεταξύ των καὶ τὸ μέτρον τους μικρότερον τοῦ ὁρίου $0.50\ \sigma_3$. Τὰ πειραματικὰ δεδομένα, τὰ ἀντιστοιχοῦντα εἰς τὴν ἀρχικήν, καθὼς ἐπίσης καὶ εἰς τὴν τελικὴν ἐπιφάνειαν διαρροῆς, εἰσήχθησαν εἰς εἰδικὸν κριτήριον τανυστικοῦ πολυωνύμου ἀστοχίας, κατάλληλον διὰ τὸν ὁρισμὸν τῶν ἐπιφανειῶν ἀστοχίας τῶν ἀνισοτρόπων ὑλικῶν. Ἐπὶ τῇ βάσει συγχρόνων ἀνταποκριτικῶν θεωριῶν, προσεγγίσαμεν τὴν ἀνισότροπον κράτυνσιν κατὰ τὴν ἐλαστοπλαστικὴν συμπεριφορὰν τοῦ πάγου μὲ ἕνα καταλλήλως ὁριζόμενον ἀνισότροπον εἰκονικὸν ἐλαστικὸν ὑλικόν, αἱ ἰδιότητες τοῦ ὁποίου ἦσαν σύμφωνοι μὲ τὰ ἰσχύοντα δεδομένα τῶν πειραμάτων διὰ τὸ ἐλαστοπλαστικὸν πεδίον φορτίσεων. Τὰ δεδομένα ταῦτα εἰσήχθησαν εἰς τὸ κριτήριον τῆς ἐλλειπτικῆς παραβολοειδοῦς ἐπιφανείας ἀστοχίας, τὸ ὁποῖον περιγράφεται μὲ τὸ ἀντίστοιχον τανυστικὸν πολυώνυμον ἀστοχίας. Εἰσάγοντες ἐν συνεχείᾳ βαθμιδωτὴν μορφὴν φορτίσεως τῶν δοκιμίων, συνάγομεν ἐπαρκῆ ἀριθμὸν δεδομένων διὰ τὸν ἀκριβῆ προσδιορισμὸν τῶν ἐπιφανειῶν ἀστοχίας εἰς τὴν ἐλαστοπλαστικὴν περιοχὴν τῆς φορτίσεως, μέχρι πλήρους καὶ ὁλοκληρωτικῆς ἀστοχίας τοῦ ὑλικοῦ.

Ἡ ἐφαρμοσθεῖσα ἀριθμητικὴ μέθοδος διὰ ταυτοποιήσεως τῶν παραμέτρων ἐξετελέσθη εἰς κατάλληλον περιβάλλον νευρωνικοῦ δικτύου, μέσῳ ἐπιτηρούμενων καὶ μὴ-ἐπιτηρούμενων ἀλγορίθμων. Τὸ δίκτυον διδάσκεται νὰ παρεμβάλῃ ἢ νὰ προσεκβάλῃ τὰ ὑπάρχοντα πειραματικὰ δεδομένα, τὰ ὁποῖα εὑρίσκονται συγκεντρωμένα εἰς τὸ τεταρτημόριον θλίψεως τοῦ ἐπιπέδου τῶν κυρίων τάσεων, ἐφ' ὁλοκλήρου τῆς ἐπιφάνειας ἀστοχίας. Ὁ ρυθμὸς συγκλίσεως τῆς ἀριθμητικῆς μεθόδου, ἐξαρτώμενος ἐκ τῆς ποσότητος τῶν πειραματικῶν τιμῶν καὶ τῆς ἀξιοπιστίας των, θεωρεῖται ὡς ἱκανοποιητικός, παρέχων ἀκριβῆ καὶ σταθερὰ ἀποτελέσματα μετὰ ἀπὸ ὀλίγους μόνον κύκλους ἐπαναλήψεων τῆς ἀριθμητικῆς προσεγγίσεως.

Ἡ περιγραφεῖσα μέθοδος ἐφηρμόσθη εἰς σειρὰν πειραμάτων θλίψεως-θλίψεως εἰς δείγματα πάγου Ι διὰ τρία διαδοχικὰ ἐπίπεδα φορτίσεως, ἀντιστοιχοῦντα εἰς διαφόρους ταχύτητας ἐπιβολῆς τῶν παραμορφώσεων καὶ προέκυψαν ἐκ τῆς μελέτης

ταύτης ἐνδιαφέροντα ἀποτελέσματα, ἀφορῶντα εἰς τὴν ἀντοχὴν καὶ εἰς τὴν διαδικασίαν ἀστοχίας αὐτοῦ τοῦ σημαντικοῦ ὑλικοῦ.

Ὁ πάγος ἀποτελεῖ ἓν ἐξόχως ψαθυρὸν ὑλικόν, συγκρινόμενον μὲ ἄλλα σχετικὰ ὑλικὰ εἰς ἀντιστοίχους στάθμας θερμοκρασίας. Ἕως τώρα, ἀρκεταὶ μελέται ἔχουν πραγματοποιηθῆ διὰ τὸν καθορισμὸν τοῦ ἑρπυσμοῦ καὶ τῆς πλαστικότητος τοῦ πάγου, ἐπειδὴ αἱ διαδικασίαι αὗται, ὡς γνωστόν, κυριαρχοῦν εἰς φύλλα πάγου ὑπὸ τὴν ἐπίδρασιν μικρῶν ἀποκλινουσῶν τάσεων. Ἐν τούτοις, ὁ τρόπος ἀστοχίας τοῦ πάγου εἰς πολυαξονικὴν καταπόνησιν εἶναι ἐξίσου σημαντικὸς διὰ τὴν γενικωτέραν μηχανικὴν συμπεριφοράν του εἰς τὰς ψαθυρὰς θραύσεις. Παρὰ τὴν σπουδαιότητα αὐτοῦ τοῦ μηχανισμοῦ ἀστοχίας, ἡ ὑπάρχουσα πειραματικὴ μελέτη εἶναι μικρὰ καὶ δὲν ὑπάρχει μέχρι σήμερον ἐπιτυχὲς κριτήριον ἀστοχίας διὰ τὸν πάγον εἰς πολυαξονικὰς φορτίσεις.

Ἐπειδὴ ἡ ψαθυρὰ θραῦσις καὶ ἀστοχία τοῦ πάγου εἶναι ἰσχυρῶς ἐξαρτώμεναι ἐκ τῆς ὑδροστατικῆς θλίψεως τοῦ πάγου, καθίσταται ἀναγκαία ἡ μελέτη τῆς ἀντοχῆς του τῇ βοηθείᾳ πολυαξονικοῦ κριτηρίου θραύσεως, τὸ ὁποῖον θὰ περιγράφῃ ὅλα τὰ χαρακτηριστικὰ τῆς ἀστοχίας αὐτοῦ τοῦ ὑλικοῦ. Ἐν συνεχείᾳ, ἡ συστηματικὴ πειραματικὴ ἐξέτασις τῶν μηχανισμῶν ἀστοχίας ὑπὸ πολυπλόκους καταστάσεις τάσεως κρίνεται ὡς ἐπιτακτικὴ διὰ τὴν περιγραφὴν τοῦ μηχανισμοῦ ἀντιστάσεως τοῦ σημαντικοῦ τούτου ὑλικοῦ. Ἐν τούτοις, πολυαξονικαὶ δοκιμαὶ ἀντοχῆς κατὰ μῆκος τῶν κυρίων διευθύνσεων τοῦ πάγου εἶναι σπάνιαι καὶ ὀλίγαι μόνον ἔχουν ἐκτελεσθῆ διὰ τὸν καθορισμὸν τῶν μηχανισμῶν ἀστοχίας τῶν διαφόρων εἰδῶν πάγου.

Ὁ Hausler (1981), καθὼς καὶ οἱ Schulson, Jones καὶ Kuehn (1991) ἐμελέτησαν τὸν πάγον ὑπὸ πολυαξονικὰς θλιπτικὰς καταπονήσεις καὶ ἑρμήνευσαν τὸ φαινόμενον αὐξήσεως τῆς ἀντοχῆς του εἰς θλιπτικὴν ἀστοχίαν ὑπὸ ψαθυρὰς συνθήκας. Ἐπιπροσθέτως, οἱ Rist καὶ Murrell (1994) ἐπραγματοποίησαν πειράματα τριαξονικῶν φορτίσεων πολυκρυσταλλικοῦ πάγου ὑπὸ θλιπτικὰς συνθήκας, εὐνοϊκὰς εἰς ψαθυρὰς θραύσεις καὶ μικρορωγμάς. Ἐμελετήθη ἡ ἐπίδρασις τῶν παραπλεύρων πιέσεων προκαλουσῶν μετρίας συσφίγξεις καὶ ἀπεδείχθη ὅτι διὰ μικρὰς τιμὰς τῶν πιέσεων συσφίγξεως ἡ ψαθυρὰ ἀντοχὴ ἦτο ἐξαρτωμένη ἐκ τῆς πιέσεως. Παρὰ ταῦτα, διὰ μεγαλυτέρας συσφίγξεις, ἀντιστοιχοῦσαν εἰς παραπλεύρως θλιπτικὰς ὑδροστατικὰς πιέσεις ἴσας μὲ $\sigma_1 = \sigma_2 \geqslant 0.15\ \sigma_3$, ἡ θραῦσις προσομοιάζει πρὸς ὁλικῶς διατμητικὴν μορφήν, ἐμφανιζόμενης λοξῆς ρωγμῆς, ἀκολουθούμενης ἐνδεχομένως ἀπὸ διακλαδώσεις καὶ δευτερευούσας ρωγμάς.

Κατὰ τὴν διάρκειαν τῶν τριαξονικῶν πειραμάτων ποὺ ἐπραγματοποιήθησαν, ἐπεβλήθη εἰς τὰ κυλινδρικὰ δείγματα πάγου πολυαξονικὴ θλιπτικὴ ἐντατικὴ κατάστασις, μὲ τὰς ἀπολύτως ὑψηλοτέρας τιμὰς τῆς θλιπτικῆς τάσεως σ_3 κατευθυνόμενας

κατὰ μῆκος τοῦ ἄξονος τῶν κυλινδρικῶν δειγμάτων, καὶ ὑπέρθεσιν ἐπ' αὐτῆς πλευρικῶς θλιπτικῆς καταστάσεως τάσεων, ὅπου $\sigma_1 = \sigma_2 < \sigma_3$.

Ὁ ὁρισμὸς τῶν τάσεων καὶ τῶν ἐπιφανειῶν διαρροῆς διὰ τὰς διαφόρους βαθμίδας φορτίσεως θεωρεῖ ὡς διαδικασίαν ἐκμαθήσεως μίαν καταλλήλως ὡρισμένην ἀριθμητικὴν διαδικασίαν, χρησιμοποιῶν τὴν μέθοδον τῶν ἐλαχίστων τετραγώνων μὲ περιωρισμένας συνθήκας, καὶ βασίζεται εἰς τὴν ἐγκυρότητα τοῦ τανυστικοῦ πολυωνύμου ἀστοχίας ἕως τὴν καταστατικὴν συνθήκην περιγράφουσαν τὴν προοδευτικὴν διαρροήν. Συνεπῶς, ἡ μέθοδος ἐπιλύσεως συνίσταται εἰς τὴν κατασκευὴν ἀριθμητικῆς μεθόδου, καταλλήλως ἐκπαιδευμένης διὰ τὴν προσομοίωσιν τῶν ὑπαρχόντων πειραματικῶν ἀποτελεσμάτων, καὶ διὰ τὴν ἐπέκτασιν τῶν ἀποτελεσμάτων αὐτῶν, λαμβάνουσα ὑπ' ὄψιν ὅλα τὰ εἰς τὸ τεταρτημόριον θλίψεως τοῦ χώρου τῶν κυρίων τάσεων δεδομένα καὶ ἐπεκτείνουσα τὰς πληροφορίας εἰς ὁλόκληρον τὸν χῶρον τῶν τάσεων. Ὁρίζονται τοιουτοτρόπως οἱ τόποι διαρροῆς τοῦ ὑλικοῦ, βασιζόμενοι εἰς μικρὸν ἀριθμὸν πειραματικῶν σημείων. Περαιτέρω, καθίσταται δυνατὸς ὁ καθορισμὸς τῶν διαδοχικῶν τόπων διαρροῆς ὡς πρὸς τὰς ἀρχικὰς πειραματικὰς ἐπιφανείας διαρροῆς, θεωρώντας ὅτι τὸ ὑλικὸν εἶναι ἐν ἐξελίξει μεταβαλλόμενον ἀνισότροπον ὑλικόν, ἡ μεταβολὴ τῆς ἀνισοτροπίας τοῦ ὁποίου ὀφείλεται εἰς τὴν ἐπιπλέον ἀνάπτυξιν τῆς πλαστικότητος τῶν ἀρχικῶς ἀναπτυσσομένων πλαστικῶν ζωνῶν. Ἐν συνεχείᾳ, ἡ διαδικασία καλεῖται νὰ μελετήσῃ τὸν νόμον μεταβολῆς τῆς ἀνισοτροπίας τοῦ ὑλικοῦ, καί, ὅταν αὐτὴ ἐφαρμοσθῇ εἰς ὅλον τὸ σύνολον τῶν πειραματικῶν δεδομένων, νὰ ἐκπληρώνῃ τὸ καθῆκον της καὶ νὰ ὁρίζῃ τὸ ἑπόμενον βῆμα εἰς συντομωτέρους χρόνους καὶ μὲ μεγαλυτέραν ἀκρίβειαν. Ἡ μέθοδος αὐτὴ δι' ἐφαρμογῆς τῆς δυνατότητος προσαρμοστικότητος τοῦ κριτηρίου τοῦ τανυστικοῦ πολυωνύμου ἀστοχίας, ἐκφραζομένου ἀπὸ ἐλλειπτικὴν παραβολοειδῆ ἐπιφάνειαν ἀστοχίας (EPFS), δύναται νὰ ὁρίσῃ τὰ ἰσοδύναμα ἐλαστικὰ χαρακτηριστικὰ ἀστοχίας δι' ἐφαρμογῆς συνεχῶς μεταβαλλομένων μορφῶν τοῦ τόπου ἀστοχίας. Αἱ λεπτομέρειαι τῆς θεωρίας αὐτῆς καὶ τῶν μεθόδων ἀριθμητικῆς ἐπιλύσεως παρουσιάζονται πλήρως εἰς προγενεστέρας ἐργασίας.

Εἶναι εὐρέως ἀποδεκτὸν τὸ γεγονὸς ὅτι, ὅταν τὸ ὕδωρ ψύχεται, εἶναι δυνατὸν νὰ σχηματίσει ποικιλίαν δομῶν. Ἡ δομὴ τῶν μορίων ἡ παρουσιαζόμενη εἰς τὸ σχῆμα 1 ἀντιστοιχεῖ εἰς πάγον I, τὸν γνώριμον πάγον ποὺ σχηματοποιεῖται καὶ εἶναι σταθερός, εἰς φυσιολογικὰς συνθήκας ἀτμοσφαιρικῆς πιέσεως. Ἐννέα διαφορετικαὶ μορφαὶ πάγου εἶναι γνωσταί, ἕκαστη τούτων ὁριζομένη ἐκ τῆς κρυσταλλικῆς της δομῆς. Μεταβολαὶ εἰς τὴν θερμοκρασίαν καὶ τὴν πίεσιν μετασχηματίζουν τὸν ἕνα τύπον πάγου εἰς ἄλλον. Αἱ μεταβολαὶ αὐταὶ εἶναι συγκεκριμέναι καὶ ἔχουν χαρτογραφηθῆ εἰς διαγράμματα φάσεως (Σχῆμα 2). Κατὰ συνέπειαν, ὁ πάγος I εἰς τοὺς -10° C μεταμορφώνεται ὑπὸ πίεσιν 4,400 atm εἰς πάγον V, ἐνῶ εἰς τὸ ἴδιον ἐπίπεδον θερμοκρα-

σίας καὶ ὑπὸ πίεσιν 6,300 atm μεταβάλλεται εἰς πάγον VI. Ὁμοίως, ὁ πάγος I εἰς -30° C μετασχηματίζεται εἰς πάγονIII εἰς 2,200 atm, λαμβανομένου ὑπόψιν ὅτι, ἐὰν ἡ πίεσις αὐξηθῆ εἰς 3,000 atm, μετατρέπεται εἰς πάγον II. Ἐπιπλέον, ὁ πάγος εἰς τοὺς -30° C μετατρέπεται περαιτέρω εἰς πάγον V καὶ πάγον VI εἰς πιέσεις μεγαλυτέρας τῶν 3,000 atm. Τὸ σχῆμα 2 παρουσιάζει τὸ διάγραμμα σχηματισμοῦ τοῦ πάγου ὡς συνάρτησιν τῶν συνδυασμῶν τῶν θερμοκρασιῶν καὶ τῶν πιέσεων κατὰ τὴν διάρκειαν τῆς διαδικασίας σχηματισμοῦ του, ὅπου αἱ καταστάσεις ἰσορροπίας ὑποδεικνύονται διὰ τοὺς σχηματισμοὺς τοῦ πάγου εἰς ὑψηλὰς πιέσεις.

Ἡ παροῦσα ἐργασία ἑστιάζεται εἰς τὴν μελέτην τῶν μηχανισμῶν διαρροῆς καὶ ἀστοχίας τοῦ πολυκρυσταλλικοῦ πάγου εἰς τὴν ὄλκιμον-ψαθυρὰν περιοχὴν παραμορφώσεων. Ἐπραγματοποιήθησαν τριαξονικὰ πειράματα θλίψεως εἰς πολυκρυσταλλικὸν κοκκώδη πάγον, εἰς σταθεροὺς ρυθμοὺς παραμορφώσεως. Ἐμελετήθη τὸ ἀποτέλεσμα τῆς τριαξονικότητος τῶν ἐξωτερικῶς ἐφηρμοσμένων φορτίων εἰς τὸν τόπον διαρροῆς καὶ ἀστοχίας τοῦ ὑλικοῦ. Ἐπειδὴ τὸ ὑλικὸν αὐτὸ συμπεριφέρεται ὡς ψαθυρὸν ὑλικόν, ἐχρησιμοποιήθη τὸ κριτήριον τῆς ἐλλειπτικῆς παραβολοειδοῦς ἐπιφανείας ἀστοχίας δι' ὀρθότροπα ὑλικά, καὶ ἐνδιαφέροντα ἀποτελέσματα καὶ συμπεράσματα συνήχθησαν ἀφορῶντα τὸν μηχανισμὸν ἀστοχίας τοῦ ὑλικοῦ αὐτοῦ ὑπὸ τὴν ἐπίδρασιν τριαξονικῆς φορτίσεως.

Ἡ κρυσταλλικὴ δομὴ τοῦ πάγου δύναται νὰ περιγραφῆ ἐξ ἑνὸς μοναδιαίου κρυστάλλου, ἐπεκτεινόμενου ἀπεριορίστως εἰς ὅλας τὰς διευθύνσεις, μὲ κάθε ἄτομον ὀξυγόνου τοποθετημένον εἰς τὸ κέντρον βάρους τῶν τεσσάρων γειτονικῶν ἰσαπεχόντων ἀτόμων ὀξυγόνου, διαχωριζόμενον ἐξ ἀτόμων ὑδρογόνου, ὥστε ἕκαστον ἄτομον ὑδρογόνου νὰ ἅπτεται δύο γειτονικῶν ἀτόμων ὑδρογόνου καὶ ἕκαστον ἄτομον ὀξυγόνου νὰ ἅπτεται τεσσάρων ἀτόμων ὑδρογόνου, συμφώνως πρὸς τὸ ὑπόδειγμα τοῦ σχήματος 1α. Τὰ τρία ἄτομα τοῦ στοιχείου δὲν εἶναι εὐθυγραμμισμένα, ἀλλὰ σχηματίζουν γωνίαν τινὰ μεταξύ των, ὥστε ἡ τρισδιάστατος δομὴ τοῦ μορίου τοῦ ὕδατος νὰ στερεῖται συμμετρίας καὶ νὰ περιέχη τέσσαρα ἀνόμοια μέλη, τοποθετημένα εἰς ἕνα ἀτελῆ κύβον. Συνεπῶς, αἱ σχηματιζόμεναι γωνίαι ἐκ τῶν δύο ἀτόμων ὑδρογόνου καὶ τοῦ ἀντιστοίχου κεντρικοῦ ἀτόμου τοῦ ὀξυγόνου εἶναι περίπου ἴσαι μὲ 105° καὶ ἡ ἀπόστασις μεταξὺ τοῦ ἀτόμου τοῦ ὀξυγόνου καὶ ἑκάστου πυρῆνος ὑδρογόνου νὰ ἰσοῦται μὲ 0.96 Å. Ἔναντι τῶν ἀτόμων ὑδρογόνου καὶ μὲ διεύθυνσιν πρὸς τὰς ἀπέναντι γωνίας τοῦ μοναδιαίου κύβου, σχηματίζονται δύο ἠλεκτρονικὰ νέφη, ὑπαίτια διὰ τὴν ἰδιόρρυθμον συμπεριφορὰν τοῦ ὕδατος, καθότι αὐτὰ ἕλκουν τὸν πυρῆνα ὑδρογόνου ἑνὸς γειτονικοῦ μορίου τοῦ νεροῦ, σχηματίζοντα κατὰ συνέπειαν νέφος ὑδρογόνου (Σχῆμα 1β).